Gastroenterology 2026;170:787–802

Overcoming CXCR4-Mediated T-Cell Exclusion Potentiates Antitumor Cytotoxicity in Fibrolamellar Carcinoma

Jason A. Carter,[1,*] **Lindsay K. Dickerson**,[1,*] **Andreas Stephanou**,[2,*] Sheela R. Damle,[3,4] Kristin E. Goodsell,[1] Sara K. Daniel,[1] Kevin M. Sullivan,[1,5] Bo Shui,[2] Xiuyun Jiang,[1] Heidi L. Kenerson,[1] Renske J. E. van den Bijgaart,[6] Alaa R. Farghli,[2] Yongjun Liu,[7] Emily Beirne,[7] Kevin P. Labadie,[1] Jack Cernak,[1] Sardar Shahmir B. Chauhan,[1] Jose Mario Bello Pineda,[8] Annalyssa N. Long,[9] Anna E. Elz,[9] Evan W. Newell,[6,9,10] Teresa S. Kim,[1] Kimberly J. Riehle,[1] Raymond S. Yeung,[1] Shreeram Akilesh,[7] Ian N. Crispe,[1,7,11] Kevin C. Barry,[6] **Praveen Sethupathy**,[2,§] and **Venu G. Pillarisetty**[1,§]

[1]Department of Surgery, University of Washington, Seattle, Washington; [2]Department of Biomedical Sciences, Cornell University College of Veterinary Medicine, Ithaca, New York; [3]Department of Medicine, University of Washington, Seattle, Washington; [4]Clinical Research Division, Fred Hutchinson Cancer Center, Seattle, Washington; [5]Department of Surgery, Louisiana State University Health Sciences Center, New Orleans, Louisiana; [6]Public Health Sciences Division, Fred Hutchinson Cancer Center, Seattle, Washington; [7]Department of Laboratory Medicine and Pathology, University of Washington, Seattle, Washington; [8]Medical Scientist Training Program, University of Washington, Seattle, Washington; [9]Immunotherapy Integrated Research Center, Fred Hutchinson Cancer Center, Seattle, Washington; [10]Vaccine and Infectious Disease Division, Fred Hutchinson Cancer Center, Seattle, Washington; and [11]Department of Immunology, University of Washington, Seattle, Washington

BACKGROUND & AIMS: Fibrolamellar carcinoma (FLC) is a rare liver cancer affecting young adults without underlying cirrhosis. Although almost all FLC patients share an immunogenic DNAJB1-PRKACA fusion oncogene, endogenous antitumor immunity and clinical response to immunotherapy are limited. We hypothesized that the lack of response to immunotherapy is mediated by both T-cell exclusion and intratumoral immunosuppression. **METHODS:** We used high-throughput single-nucleus RNA sequencing to explore the tumor immune microenvironment (TIME) of FLC. We then used multiplex immunohistochemistry, live imaging, single-cell sequencing, and spatial proteomics in a human tumor slice culture (TSC) system to dissect and experimentally modulate the FLC TIME. **RESULTS:** We identified significant dysregulation of stromal-immune signaling pathways within the FLC TIME relative to adjacent nontumor liver, notably including interactions between $CXCL12^{+}$ myofibroblasts and $CXCR4^{+}$ lymphocytes. CXCR4 inhibition was sufficient to mobilize stromal T cells into the carcinoma compartment, with the addition of PD-1 blockade independently activating T-cell antitumor effector function. Combination CXCR4 and PD-1 blockade resulted in a significant increase in tumor cell death relative to either treatment alone in a human TSC model. **CONCLUSIONS:** Our findings demonstrate that immune resistance in FLC is mediated by both local T-cell exclusion and exhaustion, with combination CXCR4 and PD-1 blockade acting cooperatively to overcome these independent mechanisms. These results highlight the versatility of the human TSC system to aid in the study of rare cancer types and provide important preclinical evidence for the rational design of combination immunotherapy in FLC, which currently lacks any effective systemic therapy.

Keywords: Fibrolamellar Carcinoma; Combination Immunotherapy; Tumor Immune Microenvironment; CXCL12.

Fibrolamellar carcinoma (FLC) is a rare, aggressive form of liver cancer in young adults that arises from otherwise healthy parenchyma, with complete surgical resection offering the only potential cure.[1] FLC patients, however, often present with advanced disease and have high rates of recurrence after surgery, with systemic chemotherapy currently offering no demonstrable survival benefit.[2,3] Case reports and retrospective studies have found inconsistent responses to immune checkpoint blockade, particularly with single-agent immunotherapy,[4–7] consistent with the low tumor mutational burden seen in FLC.[8] Given the lack of effective systemic treatments and resultant high mortality, there is an urgent need to deepen our understanding of FLC's unique tumor immune microenvironment (TIME) to aid in the development of new immunotherapeutic approaches.[9]

FLC is characterized histologically by dense bands of intratumoral stroma and molecularly by a conserved DNAJ-PKAc fusion protein that promotes aberrant protein kinase A signaling.[10–12] This fusion kinase serves as the primary oncogenic driver for FLC and as a source of targetable tumor neoantigens.[13,14] Despite the presence of these immunogenic fusion neoepitopes, intrinsic antitumor immunity in

***Authors share co-first authorship; §Authors share co-senior authorship.**

Abbreviations used in this paper: **ANTL, adjacent nontumor liver; DC, dendritic cell; FDR, false discovery rate; FLC, fibrolamellar carcinoma; HSC, hepatic stellate cell; Ig, immunoglobulin; KRT19, keratin 19; mIHC, multiplex immunohistochemistry; myCAF, myofibroblastic cancer-associated fibroblast; NK, natural killer; PDAC, pancreatic ductal adenocarcinoma; snRNAseq, single-nucleus RNA sequencing; TILs, tumor-infiltrating lymphocytes; TIME, tumor immune microenvironment; TSC, tumor slice culture.**

Most current article

0016-5085/$36.00
https://doi.org/10.1053/j.gastro.2025.10.006

WHAT YOU NEED TO KNOW

BACKGROUND AND CONTEXT

Fibrolamellar carcinoma (FLC) is a rare type of liver cancer occurring in otherwise healthy young adults that currently has no effective systemic treatment options.

NEW FINDINGS

We use an innovative human tumor slice culture system with a multi-omic approach to experimentally model the tumor immune microenvironment (TIME) in FLC. We identify CXCR4 signaling as a key driver of T-cell exclusion in FLC and show that a rationally designed combination immunotherapy strategy increases antitumor effector function.

LIMITATIONS

CXCR4 blockade mobilizes stromal T cells in a model of the human TIME. Future studies are needed to further define the role of other chemokine signaling pathways in defining the spatial distribution of immune cells in the FLC TIME.

CLINICAL RESEARCH RELEVANCE

We provide evidence for combination CXCR4 and PD-1 blockade as a new therapeutic strategy to overcome the unique and independent immunosuppressive mechanisms present in FLC. Our findings directly lay the groundwork for future immunotherapy-based clinical trials for a rare cancer type that currently does not have effective therapies.

BASIC RESEARCH RELEVANCE

We provide evidence that antitumor immunity in FLC is limited by both T-cell exclusion and immune checkpoint–mediated immunosuppression. We show that CXCR4 signaling is a key mediator in the stromal sequestration of T cells in FLC and that CXCR4 inhibition is sufficient to mobilize these lymphocytes into the carcinoma compartment. Addition of CXCR4 inhibition to PD-1 blockade cooperatively overcomes both of these independent immunosuppressive mechanisms and significantly increases antitumor immunity in our preclinical model of the human TIME.

FLC is limited. Recent examination of the FLC TIME has shown that $CD4^+$ helper and $CD8^+$ cytotoxic T cells are predominately localized to nontumor liver, liver-tumor interface, and intratumoral stromal bands.[15] Furthermore, T cells within the tumor core appear to have impaired effector function with increased markers of T-cell exhaustion.[15] This is mechanistically supported by the expression of a variety of immune-checkpoint molecules within the FLC TIME, notably including PD-1/PD-L1 in a pattern suggestive of immune-resistance.[16] FLC thus appears to create an immunosuppressive microenvironment through two independent mechanisms: T-cell exclusion from the carcinoma compartment and immune checkpoint–mediated suppression of tumor-infiltrating lymphocytes (TILs). Despite the significance of T-cell exclusion in mediating FLC tumor immune evasion, little is currently known about the molecular mechanisms that impair lymphocyte migration toward tumor cells in FLC.

Therefore, we here generated the largest FLC single-nucleus RNA sequencing dataset to date comprising 25 adjacent nontumor liver (ANTL), primary tumor, and metastatic samples. Comprehensive profiling of more than 250,000 individual nuclei across these samples revealed significant aberrations in inferred cell-cell communication within the FLC TIME, notably including a key stromal-immune interaction between the chemokine CXCL12 and its receptor CXCR4. We demonstrate that CXCL12 is highly expressed by myofibroblasts and acts locally to constrain T-cell migration out of the stroma in a keratin-19 independent manner. We then used an innovative human tumor slice culture (TSC) experimental model in combination with multiplex immunohistochemistry (mIHC), living tissue microscopy, single-cell sequencing, and spatial proteomics to show that CXCR4 inhibition mobilizes T cells from the stroma and allows for the accumulation of T cells in the carcinoma compartment. We show that PD-1 blockade works in tandem with CXCR4 inhibition through independent mechanisms to activate intratumoral T cells and ultimately increase FLC tumor cell death. Together, our findings provide mechanistic insight into FLC's immunosuppressive microenvironment, demonstrate the versatility of the human TSC model to understand treatment effects in rare tumor types, and represent an important rational basis for new immunotherapy approaches in FLC — a devastating cancer that currently has limited treatment options.

Materials and Methods

Specimen Acquisition

After obtaining informed written consent under Institutional Review Board–approved research protocols, sterile gross specimens were examined in the operating room by the operating surgeon, on-call surgical pathologist, and research team. Ensuring that tissue collection would not affect pathologic margin assessment, the surgical team procured sterile 6-mm punch biopsies of FLC tumor core, liver-tumor interface, and/or ANTL. Live tissue for TSC was placed in ice-cold Belzer UW Storage Solution (Bridge to Life Ltd.). Additional tumor samples were placed in RNAlater Stabilization Solution (Thermo Fisher Scientific, AM7021) and immediately flash frozen or fixed in 10% formalin.

Tumor Slice Culture

As previously described,[17–20] 250-μm–thick slices were sequentially cut from tumor cores using a vibratome (Leica VT 1200S) and cultured in RPMI-based media on permeable polytetrafluoroethylene membrane inserts (MilliporeSigma, PICM01250). TSCs were incubated overnight at 37°C and 5% CO_2 before treatment with 20 μg/mL immunoglobulin (Ig) G1 isotype control (BD Biosciences, 553447), 20 μg/mL of IgG1 plus 100 μg/mL of AMD3100 (Sigma Aldrich, A5602), 20 μg/mL of PD-1 blocking antibody (αPD-1, BD Biosciences, 562138), or combination therapy. Slices were incubated for 3–6 days as indicated for each experiment and had media changed when applicable on day 3. Each TSC experiment represents a distinct FLC resection with at least 3 tumor slices used for each treatment.

Slice Culture Living Tissue Microscopy

Untreated TSCs were incubated with 10 μg/mL Alexa 405 CK7 antibody (Novus Biologicals NBP2-47944AF405) and 10 μg/mL Alexa 488 CD3 antibody (BioLegend 300415) for 2 hours at 37°C and washed. Slices were transferred into an 8-well culture slide (Ibidi) with fresh, warmed media containing SR-FLICA Caspase 3/7 reagent (ImmunoChemistry) according to the manufacturer's protocol. Three-dimensional time-lapse live imaging was performed using a Leica SP8X confocal laser scanning microscope (Leica Microsystems) and a covered stage top incubator (PeCon). Imaging was carried out for at least 20 minutes before and 60 minutes after treatment. Image processing and 3D cell-tracking was performed on Imaris software (Bitplane USA).

Single-Nucleus and Single-Cell RNA Sequencing

For single-nuclei RNA sequencing experiments, combinatorial barcoding and library preparation was performed according to the manufacturer's protocol (Parse Bio). Single-cell sequencing of TSCs after 3 days of treatment was performed using the Chromium Fixed RNA Profiling Kit and 10X Chromium Controller (10x Genomics). Sequencing was performed using either the NovaSeq 6000 or NextSeq platforms (Illumina). Both datasets were processed according to current bioinformatic best practices (see Supplementary Methods).

Results

Characterization of the Fibrolamellar Carcinoma Microenvironment at Single-Nucleus Resolution

We and others have recently used multi-omic approaches with the goal of better understanding the unique genetic landscape of FLC tumor cells, however, the dynamic interplay between tumor, stromal, and immune cells within the local TIME has not been well characterized.[21–24] To address this, we generated a first-of-its-kind single-nucleus RNA sequencing (snRNA-seq) dataset encompassing 255,639 high-quality nuclei from 9 ANTL, 9 primary (8 paired), and 7 metastatic FLC samples from a total of 14 patients (Figure 1*A*, Supplementary Table 1). We identified 4 major cell type clusters, corresponding to the expected epithelial, immune, endothelial, and other mesenchymal populations (Figure 1*B*, Supplementary Figure 1). Reassuringly, differentially expressed genes between malignant and ANTL samples were relatively conserved between our dataset (pseudobulk) and prior bulk RNA sequencing data[25] (Pearson $r = 0.63$ for all genes, $r = 0.94$ for differentially expressed genes, Figure 1*C*). Similarly, a previously published FLC gene signature[22] from bulk RNA sequencing data separated ANTL and malignant samples (Figure 1*D*), establishing the reliability of the snRNA-seq dataset for further analysis.

Subclustering of the epithelial cluster demonstrated that ANTL samples, as expected, primarily contained hepatocytes and the highest relative fraction of cholangiocytes whereas primary and metastatic samples had large tumor cell populations defined by their expression of known FLC tumor markers[26–28] (Figure 1*E*). Hepatic stellate cells (HSCs) were found in both ANTL and tumor samples, with primary and metastatic tumor samples additionally containing significantly higher numbers of HSCs undergoing transdifferentiation into FAP^+ cancer-associated myofibroblasts (myCAF), in line with FLC's characteristic intratumoral fibrosis (Figure 1*F*). Similarly, ANTL endothelial cells included a distinct liver sinusoidal endothelial cell population whereas both primary and metastatic FLC exhibited significantly greater relative abundance of venous, arterial, and lymphatic endothelial cells (Figure 1*G*). Although immune cells were relatively rarer in the FLC TIME, careful immunophenotyping revealed distinct myeloid populations including macrophages, Kupffer cells, dendritic cell (DC) subpopulations, and mast cells (Figure 1*H*). Lymphocytes clearly divided into a relatively large $CD3^+$ T-cell population, as well as rare regulatory T cell, natural killer (NK) cell, and B-cell populations (Figure 1*H*). Overall, this dataset represents a valuable resource and highlights the rich heterogeneity of the FLC TIME.

Altered Chemokine Signaling Pathways in Fibrolamellar Carcinoma Implicate CXCL12 and CXCR4

We next compared cell-cell communication patterns between ANTL and either primary or metastatic FLC samples. Given the small number of cells captured for certain cell types, we generalized our annotations to include consensus clusters for DCs (conventional, plasmacytoid, regulatory), macrophages (macrophage, Kupffer cells), endothelial cells (venous, arterial, liver sinusoidal endothelial cells, lymphatic endothelial cells), vascular mural cells (pericytes, vascular smooth muscle cells), and hepatocytes (hepatocyte, mixed). We first compared pairwise cell-cell communication strength between these cell types, identifying that the myCAF and tumor cell populations were the largest source of differential signal strength in primary tumors relative to ANTL (Figure 2*A*). To better understand what pathways were altered in the FLC TIME, we then calculated the distance between signaling pathways in ANTL and primary tumor samples and notably identified differential use of signaling pathways involved with fibrosis (eg, growth differentiation factors, activin, protease-activated receptors), as well chemokine signaling (eg, CXCL family chemokines, chemerin, leukemia inhibitory factor receptor; Figure 2*B*).

We similarly compared cell-cell communication in metastatic FLC samples relative to ANTL, again identifying tumor cells and myCAFs as the primary sources of differential interaction strengths across these samples (Figure 2*C*). Pathway analysis notably suggested up-regulation of cell proliferation pathways (WNT, EGF, FGF) and, among immune-related pathways, appeared to strongly up-regulate CXCL signaling within metastatic tumors (Figure 2*D*). Although other pathways showed changes of greater magnitude in FLC, the CXCL pathway appeared to have the strongest immune-related up-regulation in both primary and metastatic FLC samples. Given that CXCR4 signaling is a key mediator of immune migration through its primary ligand

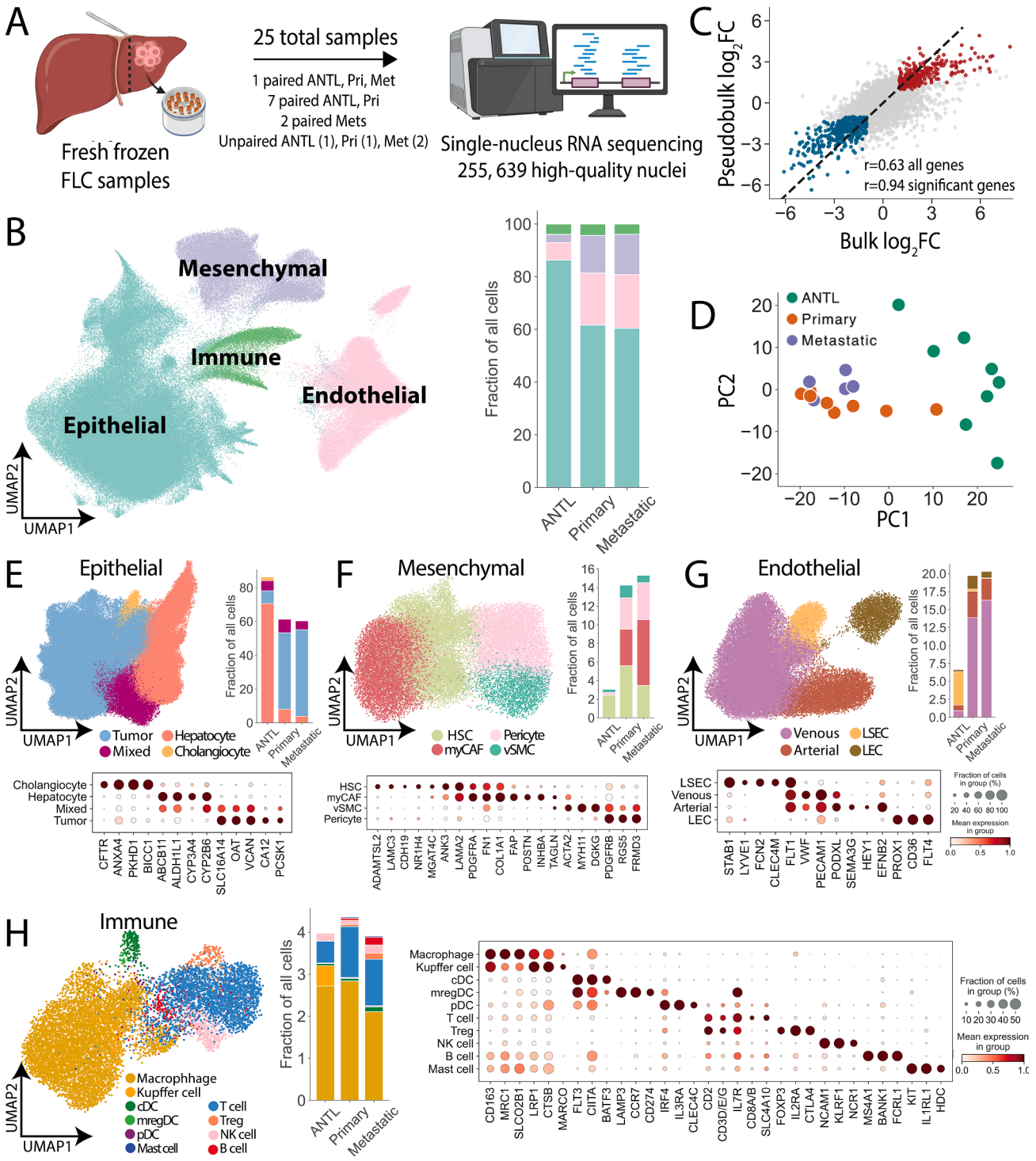

Figure 1. snRNAseq highlights the heterogeneity of the FLC TIME. (*A*) Schematic overview of snRNAseq workflow. Created with BioRender.com. (*B*) UMAP plot for 255,639 cells by major cell type (*left*) and frequency across all ANTL, primary, and metastatic samples (*right*). (*C*) Regression plot showing $\log_2$ FC between normal and primary tumor samples for pseudobulk snRNAseq data and previously published FLC bulk sequencing.[22] DGE ($P < .01$ after correction for multiple hypothesis testing) in both datasets are shown in *red* (up-regulated in primary tumors relative to ANTL) and *blue* (down-regulated in primary tumors). PC1 variance 49%, PC2 variance 11%. (*D*) PCA for ANTL, primary, and metastatic tumor samples with at least 1000 total cells using genes included in a previously published FLC signature.[22] (*E*) UMAP plots, frequency barplot, and representative marker genes showing cell subtypes within the epithelial, (*F*) mesenchymal, (*G*) endothelial, and (*H*) immune populations. *E* and *F* share the same size and color legend as *G*. cDC, conventional dendritic cell; DGE, differentially expressed genes; FC, fold change; HSC, hepatic stellate cell; LEC, lymphatic endothelial cell; LSEC, liver sinusoidal endothelial cell; Met, metastatic tumor; mregDC, mature dendritic cell enriched in immunoregulatory molecules; myCAF, cancer associated myofibroblast; NK cell, natural killer cell; PC, principal component; PCA, principal component analysus; pDC, plasmacytoid dendritic cell; Pri, primary tumor; Treg, regulatory T cell; UMAP, Uniform Manifold Approximation and Projection; vSMC, vascular smooth muscle cell.

CXCL12 in other tumor types,[29,30] we hypothesized that CXCL12-CXCR4 signaling could similarly contribute to immune exclusion in FLC. We, therefore, next specifically inferred the strength of CXCL12-CXCR4 interactions in ANTL, primary, and metastatic samples. Although HSCs were predicted to interact with both T cells and DCs in ANTL through CXCL12-CXCR4, this interaction was weaker than what is observed in primary tumors between myCAFs and T cells, B cells, DCs, and mast cells in primary tumors (Figure 2*E*, Supplementary Figure 2). Furthermore, metastatic tumors had significant dysregulation of CXCL12-CXCR4 signaling originating from myCAFs and to a lesser extent endothelial cells and macrophages (Figure 2*E*). Together, these data suggest the existence of altered chemokine signaling pathways in FLC, notably including the CXCL12-CXCR4 axis as a potential mechanism for T-cell exclusion in FLC.

$CD3^+$ T Cells are Preferentially Located Near $CXCL12^+$ Stromal Cells

Prior studies have shown the importance of chemotactic CXCL12-CXCR4 signaling axis for lymphocyte homing and modulation of T-cell tumor infiltration in other cancer types.[31–33] In pancreatic ductal adenocarcinoma (PDAC) and other tumor types, CXCL12 is produced by stromal fibroblasts but captured onto tumor cells expressing a keratin 19 (KRT19) coat that impairs migration toward tumor cells through a dimeric form of CXCL12.[34–36] As prior studies have found that only ∼20% of FLC tumors have even focal KRT19 expression,[37,38] we first asked where CXCL12 is located within primary FLC tumors by multiplex immunofluorescent imaging. In contrast to PDAC, we did not identify detectable KRT19 or CXCL12 on FLC tumor cells (Figure 3*A*; n = 4/4). Interestingly, cholangiocytes were strongly positive for both KRT19 and CXCL12, with CXCL12 expression additionally seen in endothelial cells that lacked KRT19 (Figure 3*B*). We also saw that CXCL12 expression was additionally present in stromal cells and appeared to be enriched in areas of high $CD3^+$ T-cell density at the liver-tumor interface, consistent with a KRT19-independent CXCL12-CXCR4 interaction between stromal cells and lymphocytes (Figure 3*B*).

Given T cells in primary FLC tumors are characteristically concentrated at the liver-tumor interface and within intratumoral stromal bands devoid of carcinoma cells,[15] we further explored this potential colocalization between $CXCL12^+$ stromal cells and T cells. We first annotated liver (L), interface (I), and tumor (T), as well as the intratumoral stroma (S) and carcinoma (C) compartments with an expert liver pathologist (Figure 3*C*). We used in situ hybridization to examine CXCL12 expression at the RNA level, confirming enrichment of CXCL12 transcript production at the liver-tumor interface and within stromal bands (Figure 3*D*). Immunohistochemical costaining for CD3 and CXCL12 displayed a clear spatial relationship within stromal areas, consistent with myCAFs representing the highest producers of stromal CXCL2 by snRNAseq (Figure 3*E* and *F*). Objective image analysis showed that $CXCL12^+$ cells had a greater number of $CD3^+$ cells within 50 μm when compared with $CXCL12^-CD3^-$ cells (Figure 3*G*; $P = 6.0 \times 10^{-4}$ by paired *t* test; n = 8 primary tumors). These results suggest that the myCAF–T-cell interaction mediated by CXCL12-CXCR4 may be a key contributor to T-cell exclusion.

CXCR4 Blockade Enhances Anti–PD-1 Immunotherapy in a Human Fibrolamellar Carcinoma Tumor Slice Culture Model

Building on the observed correlation between T-cell sequestration and stromal CXCL12 expression, as well as our prior findings that lymphocytes successfully infiltrating into the carcinoma compartment face a locally immunosuppressive microenvironment,[15] we predicted that combining CXCR4 with PD-1 blockade could be an effective immunotherapeutic approach for FLC. Cotreatment with CXCR4 and PD-1 blockade has been shown to be effective at mobilizing and activating T cells in other tumor types,[36,39] however, this has not previously been demonstrated in FLC. We have additionally shown that a human TSC model[17–20] can be applied to FLC patient samples, allowing for the experimental study of the FLC TIME's response to immunotherapy.[15]

We obtained FLC primary tumor (n = 7) or regional lymph node metastases (n = 2) from independent operative resections involving 7 patients and created human TSCs using these samples (Supplementary Table 2). We then treated TSCs with either a control IgG1 isotype antibody, IgG1 control with the highly specific CXCR4 inhibitor AMD3100,[40] a PD-1 blocking antibody (αPD-1), or combination therapy (Figure 4*A*). After 6 days of treatment, we used cleaved caspase-3 staining to assess the efficacy of each treatment in inducing tumor cell death[17–20] (Figure 4*B*). Relative to IgG1 control, we found that both AMD3100 and αPD-1 monotherapy significantly increased apoptosis in the carcinoma compartment (mean 30% apoptosis vs 37% and 41%, respectively, with $P = .002$ for each by paired *t* test). Combination therapy demonstrated an additive effect (52% apoptosis in the combination group, $P = 3 \times 10^{-5}$, .001, and .002 by 1-way analysis of variance relative to IgG, AMD3100, and αPD-1 monotherapies, respectively; Figure 4*C*). The effects of both monotherapies and combination treatment were similar across primary FLC and metastatic lymph node samples, as well as patients receiving prior systemic therapy (Supplementary Figure 3). Of note, our findings that FLC tumor cells had no detectable expression of CXCR4 (Figure 3*F*) and that AMD3100 monotherapy resulted in only a modest increase in apoptosis strongly suggest CXCR4 blockade is not directly cytotoxic to tumor cells. Overall, these results demonstrate that combination CXCR4 and PD-1 blockade significantly increased tumor cell death in a human TSC model and suggest that these treatments target independent mechanisms that each impede antitumor immunity.

CXCR4 Blockade Mobilizes T Cells From Stroma to Carcinoma

Our data demonstrated that stromal CXCL12 expression may mediate T-cell sequestration via its interactions with

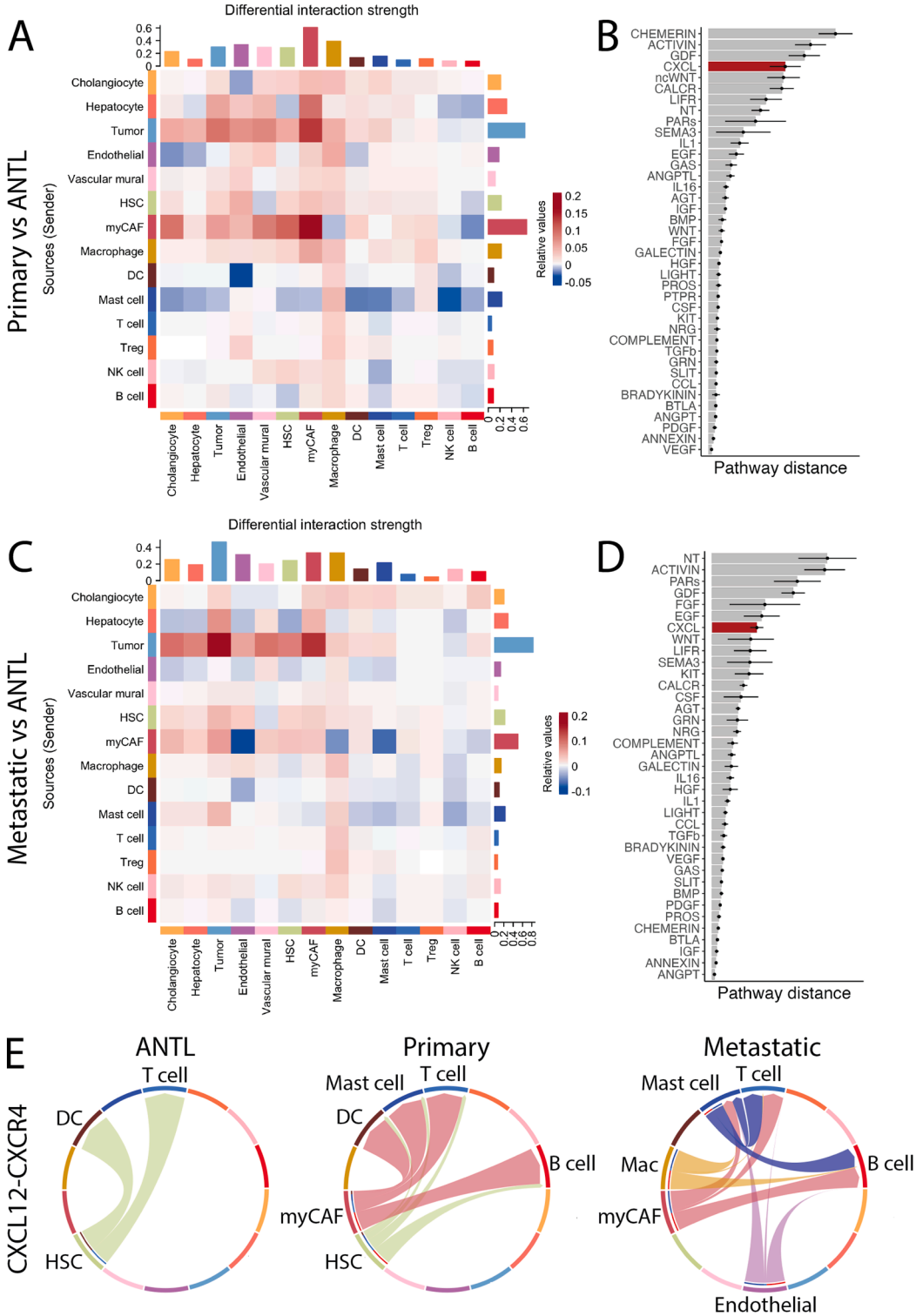

Figure 2. Altered chemokine signaling pathways between ANTL and FLC. (*A*) Cell-cell communication analysis showing pairwise differential interaction strength for cell types across primary FLC tumors (*red*) and ANTL (*blue*). (*B*) Differential pathway signaling use shown as the distance between primary FLC tumors and ANTL in joint embedding. (*C*) Heatmap showing differential interaction strength and (*D*) signaling pathway distance comparing metastatic FLC and ANTL samples. For (*B*) and (*D*), error bars represent bootstrapped standard deviation and the CXCL signaling pathway is highlighted in *red*. (*E*) Chord diagrams highlighting statistically significant CXCL12-CXCR4 interactions in ANTL (*left*), primary tumor (*middle*), and metastatic samples (*right*).

CXCR4 and that blockade of this interaction using AMD3100 results in increased tumor apoptosis. We thus predicted that the observed increase in tumor cell death was directly related to increased T-cell migration into the carcinoma compartment enabled by CXCR4 blockade. Given the high overall rate of apoptosis in TSCs after 6 days of treatment (Figure 4*C*), we chose to assess the biological impact of CXCR4 blockade and αPD-1 after 3 days when we anticipated that immune effector function would be closer to its peak (Supplementary Figure 4). We first performed mIHC on FLC TSCs treated for 3 days (n = 5; Figure 5*A*) to directly examine the impact of CXCR4 and PD-1 blockade on T-cell migration. TSCs treated with AMD3100, either alone or in combination with αPD-1, were found to have a significantly higher percentage of T cells located within the carcinoma compartment when compared with IgG1 control ($P = .05$ and $P = .03$ by paired *t* test, respectively) and αPD-1 monotherapy ($P = .05$ and $P = .01$, respectively). Addition of PD-1 blockade to AMD3100 did not increase the percentage of T cells within the carcinoma compartment compared with CXCR4 blockade alone (Figure 5*B*).

To confirm that CXCR4 blockade increases the number of T cells within the carcinoma compartment by promoting migration out of the stroma, we next used time-lapse living tissue microscopy for 1 hour before and after each treatment. We observed that T-cell migration significantly increased within the first hour after combination CXCR4 and PD-1 blockade. Quantifying pre- and post-treatment $CD3^+$ T-cell movement in a total of 4 high-power fields from 2 independent primary TSC samples revealed a statistically significant increase in the mean T-cell track length ($P = .03$ by paired *t* test) and a trend toward increased total T-cell displacement ($P = .09$) after combination CXCR4 and PD-1 blockade (Figure 5*C*–*E*). Together, these findings indicate that CXCR4 blockade induces rapid mobilization of stromal T cells into the carcinoma compartment.

PD-1 Blockade Increases Tumor-Infiltrating Lymphocyte Effector Function

To further explore the functional impact of increased T-cell migration into the carcinoma compartment, we next used mIHC to compare granzyme B expression across treatment conditions (Figure 6*A*). Quantitative analysis of mIHC from 5 TSC experiments each treated for 3 days demonstrated that both αPD-1 and combination therapy significantly increased the total percentage of cells that were granzyme B–positive throughout the TSC, including in both stroma and carcinoma compartments (2.3% and 3.5% vs 1.0% IgG1; $P = .03$ and $P = .01$ by paired *t* test, respectively). No increase in granzyme B was observed after treatment with AMD3100 alone (Figure 6*B*). Restricting this analysis specifically to the carcinoma compartment, we found that combination treatment significantly increased the percentage of granzyme B^+ $CD3^+$ T cells ($P = .01$ by paired *t* test). Treatment with αPD-1 monotherapy also appeared to increase the percentage of granzyme B^+ $CD3^+$ T cells, although this result did not achieve statistical significance ($P = .06$ by paired *t* test). Combination therapy appeared to have at least an additive effect relative to AMD3100 or αPD-1 monotherapy (Figure 6*C*).

We next used living tissue microscopy to assess the functional impact of these activated intratumoral T cells (Figure 6*D*). Again using slices taken from 2 primary resections (Supplementary Table 2), we found that combination treatment with CXCR4 and PD-1 blockade resulted in a significant increase in the fraction of $CD3^+$ T cells within 20 μm of apoptotic (cleaved caspase-3^+) tumor cells within the first hour of treatment relative to pretreatment slices ($P = .006$ by paired *t* test; Figure 6*E*). These findings together suggest that PD-1 checkpoint inhibition enhances T-cell granzyme B expression throughout the tumor microenvironment. By increasing effector function, PD-1 immunotherapy works in concert with CXCR4–blockade-induced mobilization of stromal T cells to increase the number of activated intratumoral lymphocytes and ultimately result in tumor cell death.

CXCR4 and PD-1 Blockade Mediate Complimentary but Independent T-Cell Programs

The impact of these therapies within the FLC TIME was further assessed using the Nanostring PanCancer Immune Profiling Panel[41] to analyze 5 human TSC experiments after 3 days of treatment. Differential gene expression analysis revealed that, when compared with IgG1-treated controls, combination therapy resulted in significant up-regulation of genes associated with tumor immune infiltration, T- and NK cell effector function, and tumor suppression. Genes associated with tumor function and tumor-promoting inflammation were found to be down-regulated after combination therapy (Supplementary Table 3). Differential gene expression analysis further suggested increased immune effector function and T-cell infiltration after combination therapy when compared with αPD-1 or AMD3100 monotherapy, respectively (Supplementary Table 4). Similar analysis of αPD-1 monotherapy revealed increased NK and lymphocyte activation markers relative to IgG1 control, whereas AMD3100 monotherapy resulted in no significant changes in gene expression (Supplementary Table 5; $P < .05$).

Effector function within the FLC TIME after CXCR4 and PD-1 blockade was further assessed using high-throughput, droplet-based single-cell sequencing. We obtained a total of 6483 single-cell transcriptomes from dissociated human TSCs (Patient 5; Supplementary Table 2) treated for 3 days (Figure 7*A*, Supplementary Figure 5). Focusing our analysis on immune function within cytotoxic T cells, we performed gene set enrichment analysis[42] with the goal of identifying gene sets that were up-regulated by CXCR4 or PD-1 blockade relative to control. For example, we found that genes associated with immune response regulation (GO:0046651) were enriched in $CD8^+$ cytotoxic T cells after treatment with αPD-1 monotherapy (false discovery rate [FDR] = 1.4×10^{-2}) and combination therapy (FDR =

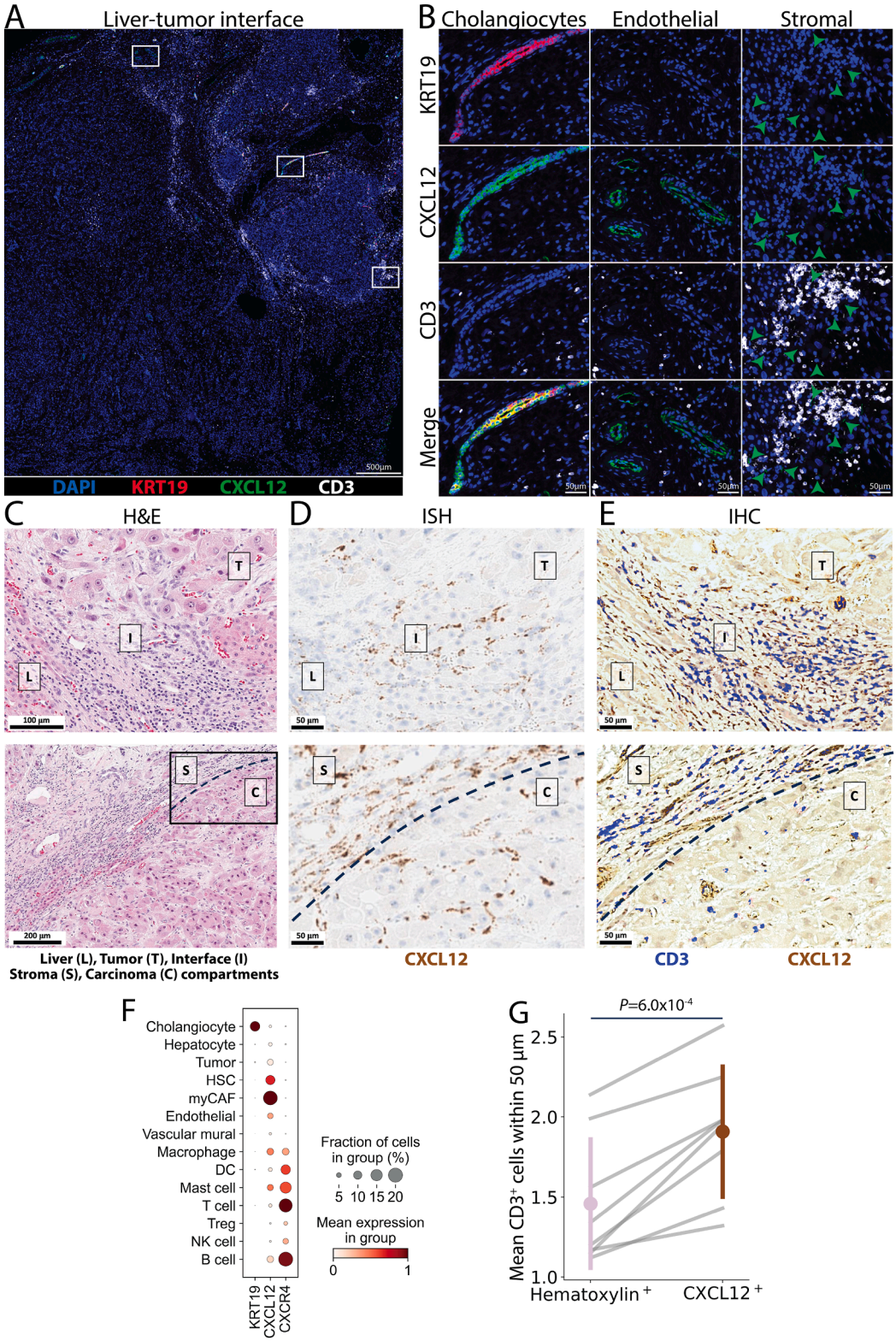

Figure 3. CD3$^+$ T cells colocalize with CXCL12 in the FLC TIME. (*A*) Representative mIF showing expression of KRT19 (*red*), CXCL12 (*green*), and CD3 (*white*). (*B*) CXCL12 expression was observed on KRT19$^+$ cholangiocytes (*left*), as well as KRT19$^-$ endothelial cells (*middle*) and stromal cells (*right*). High magnification regions of interest correspond to boxed areas in (*A*). *Green arrows* highlight selected CXCL12$^+$ stromal cells (*right*). (*C*) Representative images of H&E-stained samples showing nontumor liver (L), FLC tumor (T), and liver-tumor interface (I) (*top*), as well as the intratumoral stroma (s) and carcinoma (c) (*bottom*). (*D*) In situ hybridization showing RNA expression of CXCL12 (*brown*). (*E*) IHC staining demonstrating colocalization of CXCL12 expressing cells (*brown*) with CD3$^+$ T cells (*blue*). The stroma-carcinoma interface (*bottom*) is a magnified area represented by the box in (*D*). (*F*) Dotplot showing expression of KRT19, CXCL12, and CXCR4 by cell type from snRNAseq dataset (Figure 1). (*G*) Quantitative proximity analysis of CXCL12$^+$ and CD3$^+$ cells within intratumoral regions demonstrated a higher average number of CD3$^+$ T cells within 50 μm (n = 8). Error bars represent standard deviation and *P* values are reported from paired student *t* test. IHC, immunohistochemistry.

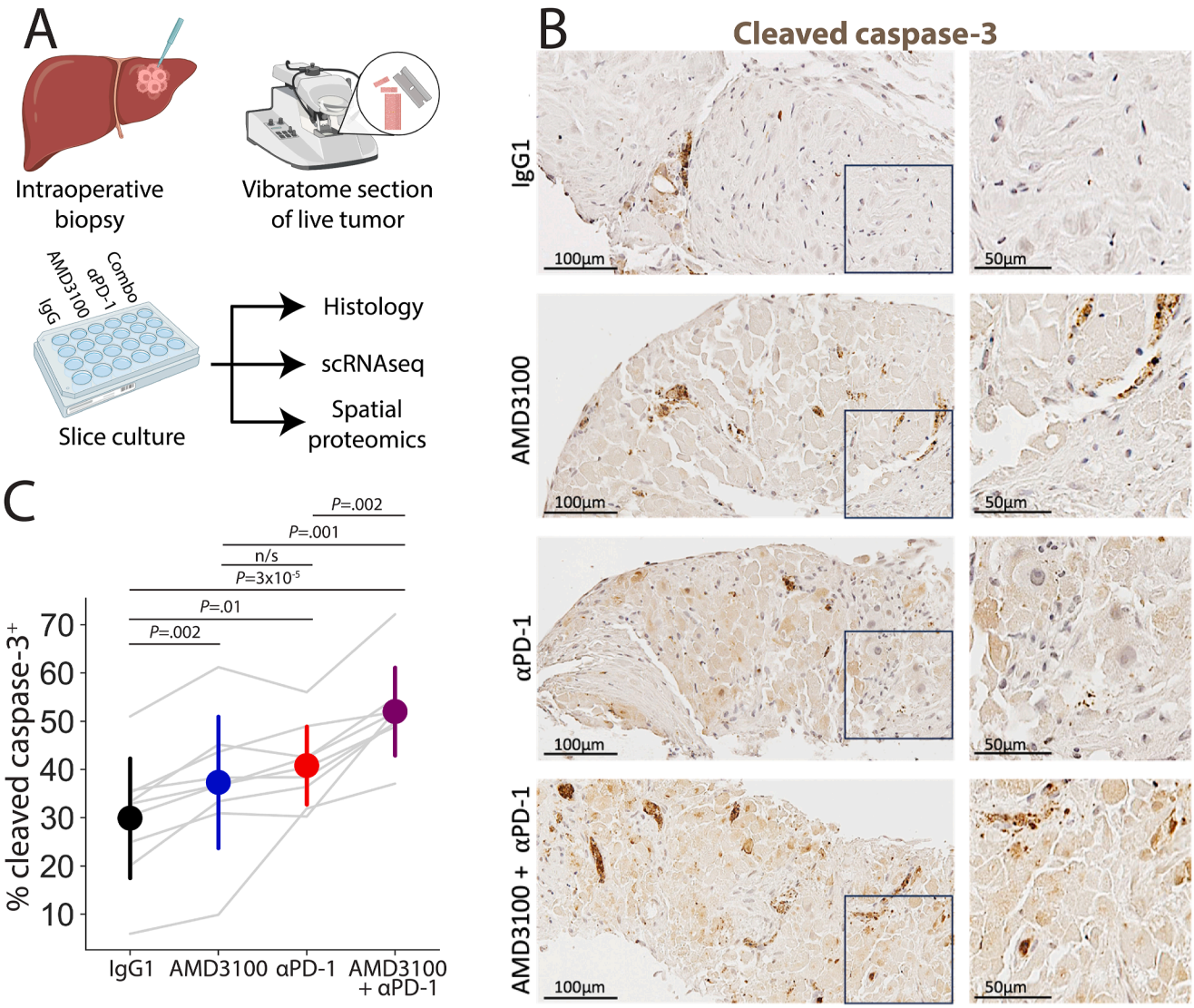

Figure 4. Combination CXCR4 and PD-1 blockade increases tumor cell death. (*A*) Schematic overview of TSC platform. Created with BioRender.com. (*B*) Representative IHC images show FLC expression of CC3, a marker of apoptosis, for control IgG1, AMD3100 (CXCR4 inhibitor), PD-1 blockade (α PD-1), and combination AMD3100 and α PD-1 treatment groups after 6 days. Higher magnification images (*right*) correspond to the boxed area for each treatment group. (*C*) Quantification of the percentage of apoptotic ($CC3^+$) cells for each treatment group (n = 9). Each individual data point is the average of 2–3 replicates and *gray lines* indicate tumor slices obtained from the same patient. Error bars represent standard deviation and *P* values are reported from 1-way ANOVA. ANOVA, analysis of variance; CC3, cleaved caspase 3.

7.5×10^{-5}), but not with AMD3100 monotherapy (Figure 7*B*). Conversely, the positive regulation of a chemotaxis-associated gene set (GO:0050921) was seen in $CD8^+$ T cells after treatment with AMD3100 alone (FDR = 3.9×10^{-5}) or in combination with αPD-1 (FDR = 6.7×10^{-3}), but not with PD-1 blockade alone (Figure 7*C*). We then searched for immune-related gene sets that were similarly up-regulated in our treatment groups. In both $CD8^+$ cytotoxic and $CD4^+$ helper T cells, we found that treatment with AMD3100 up-regulated gene sets involved in lymphocyte migration, regulation of chemotaxis, and chemokine-related signaling (Figure 7*D* and *E*). We further found that treatment with αPD-1 up-regulated gene sets associated with immune effector processes, antigen receptor-mediated signaling, and the regulation of cytokine signaling in both $CD8^+$ cytotoxic and $CD4^+$ helper T cells (Figure 7*D* and *E*).

To directly visualize the spatial impact of CXCR4 and PD-1 blockade on TILs, we next performed high-resolution spatial proteomics using the CosMx human immuno-oncology panel. We examined TSCs from 1 primary FLC sample (Patient 1; Supplementary Table 2) and treated with IgG1, AMD3100, αPD-1, or combination therapy for 3 days (n = 3 slice replicates per condition). Consistent with our prior analysis, we found $CD4^+$ and $CD8^+$ T cells localized in the stroma with minimal TILs present in TSCs treated with IgG1 control. Treatment with AMD3100 increased the number of $CD8^+$ T cells within the carcinoma compartment; however, few of these infiltrating T cells expressed granzyme A. Consistent with increased T-cell

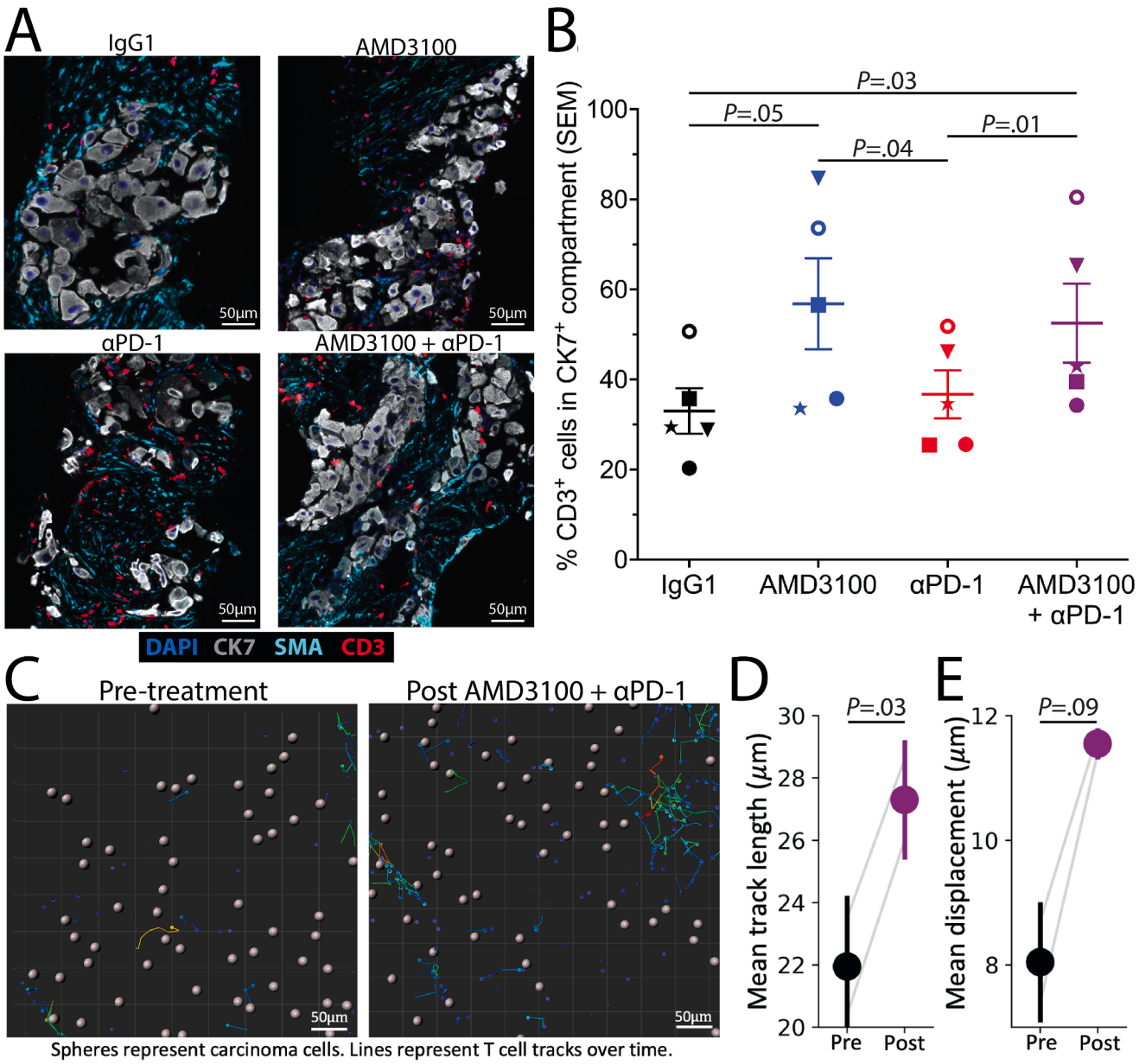

Figure 5. CXCR4 inhibition increases T-cell migration into the carcinoma compartment. (*A*) Representative mIHC images demonstrating $CD3^+$ T-cell (*red*) migration from the SMA^+ stroma (*cyan*) toward cytokeratin 7 ($CK7^+$) tumor cells (*gray*, $DAPI^+$ nuclei shown in *blue*) after 3 days of culture with control IgG1, CXCR4 inhibition (AMD3100), PD-1 blockade (α PD-1), and combination treatment. (*B*) Quantification of mIHC images demonstrates an increased percentage of $CD3^+$ T cells in the carcinoma compartment in treatment groups containing AMD3100 relative to IgG1 and α PD-1. Symbols correspond to 5 independent FLC specimens; each symbol value denotes the mean value of 3 TSC replicates per treatment group. (*C*) Living tissue microscopy T cell tracks before (*left*) and 1 hour after treatment (*right*) demonstrated (*D*) increased mean track length and (*E*) mean displacement after treatment with combination CXCR4 and PD-1 blockade from 2 TSC experiments.

activation, PD-1 blockade increased the number of stromal $CD4^+$ and $CD8^+$ T cells expressing granzyme A. However, PD-1 monotherapy resulted in a relatively limited increase in the number of intratumoral T cells despite the increased markers of activation, thereby limiting the overall antitumor effect. Spatial proteomic analysis further demonstrated the additive effect of combination blockade, with dual CXCR4 and PD-1 blockade resulting in both an increased number and enhanced activation of intratumoral T cells (Figure 7*F*). These findings are consistent with the known mechanisms of CXCR4 and PD-1 blockade and demonstrate the distinct and potentially synergistic effects of combination treatment in overcoming T-cell exclusion and intratumoral exhaustion in FLC.

Discussion

Despite recent evidence for the immunogenicity of the *DNAJB1-PRKACA* fusion sequence in FLC,[13,14] the endogenous immune response against FLC is limited and immune

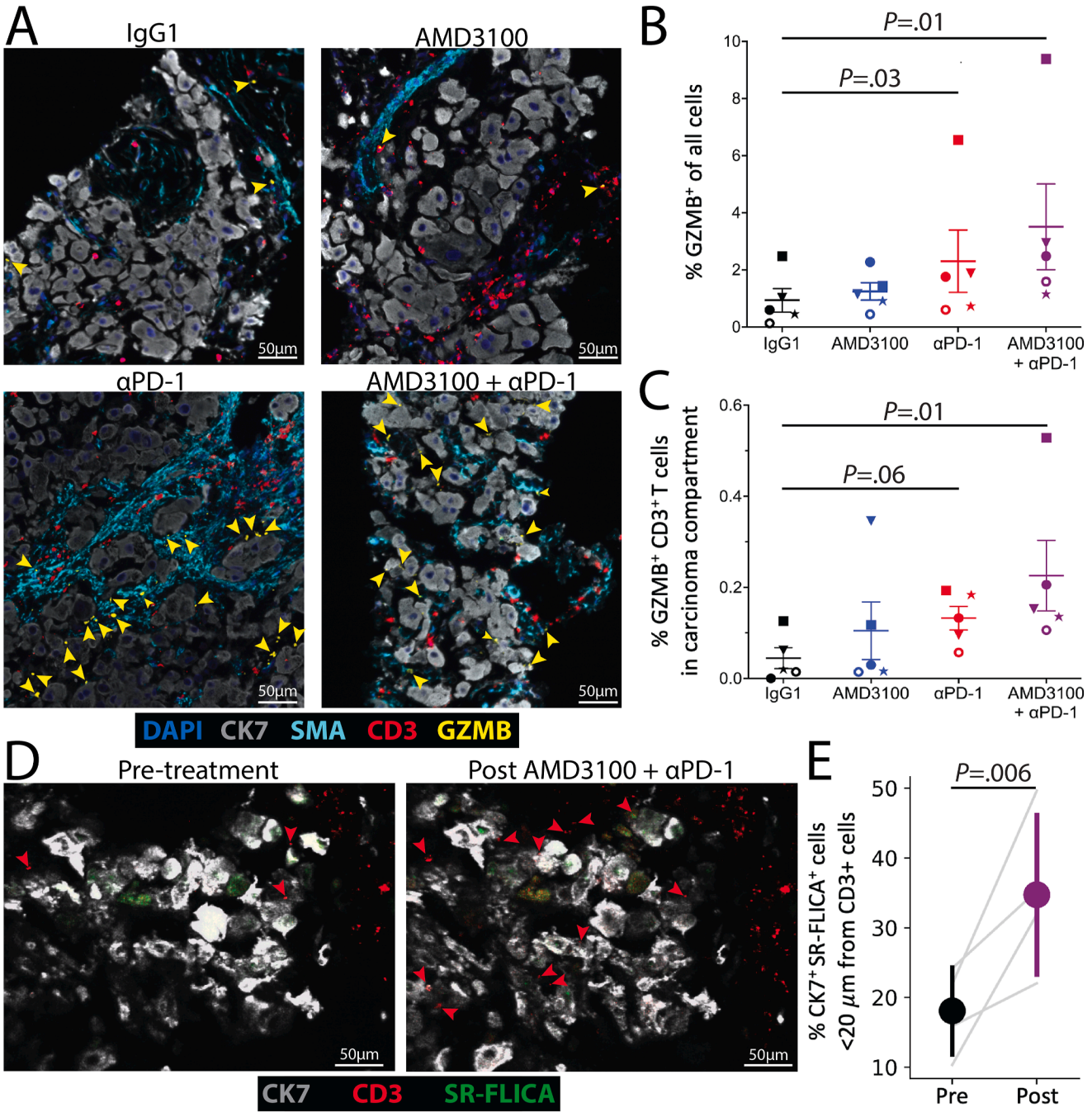

Figure 6. PD-1 blockade increases T-cell activation in FLC. (*A*) Representative mIHC images demonstrating GZMB expression in FLC TLCs after 3 days of treatment with control IgG1, CXCR4 inhibition (AMD3100), PD-1 blockade (α PD-1), or combination treatment. DAPI (nuclei), *blue*; $CK7^+$ tumor cells, *gray*; SMA^+ stromal cells, *cyan*; $CD3^+$ T cells, *red*; and GZMB, *yellow*. *Yellow arrowheads* highlight selected areas of GZMB expression. (*B*) Percentage of $GZMB^+$ cells of all cells (n = 5) and (*C*) percentage of $GZMB^+CD3^+$ cells of all cells in the carcinoma compartment. (*D*) Representative snapshot of time-lapse imaging showing $CD3^+$ T cell (*red*) migration toward $CK7^+$ tumor cells (*gray*) with apoptosis denoted by SR-FLICA staining (*green*). *Red arrowheads* highlight selected tumor-adjacent $CD3^+$ lymphocytes. (*E*) Apoptotic carcinoma cells colocalize with T cells on living tissue microscopy after combination therapy, demonstrated by percentage of $CK7^+$SR-$FLICA^+$ cells <20 μm from $CD3^+$ cells (n = 4 high-powered fields from 2 TSC experiments). Error bars represent standard deviations with *P* values reported by paired *t* test. GZMB, granzyme B.

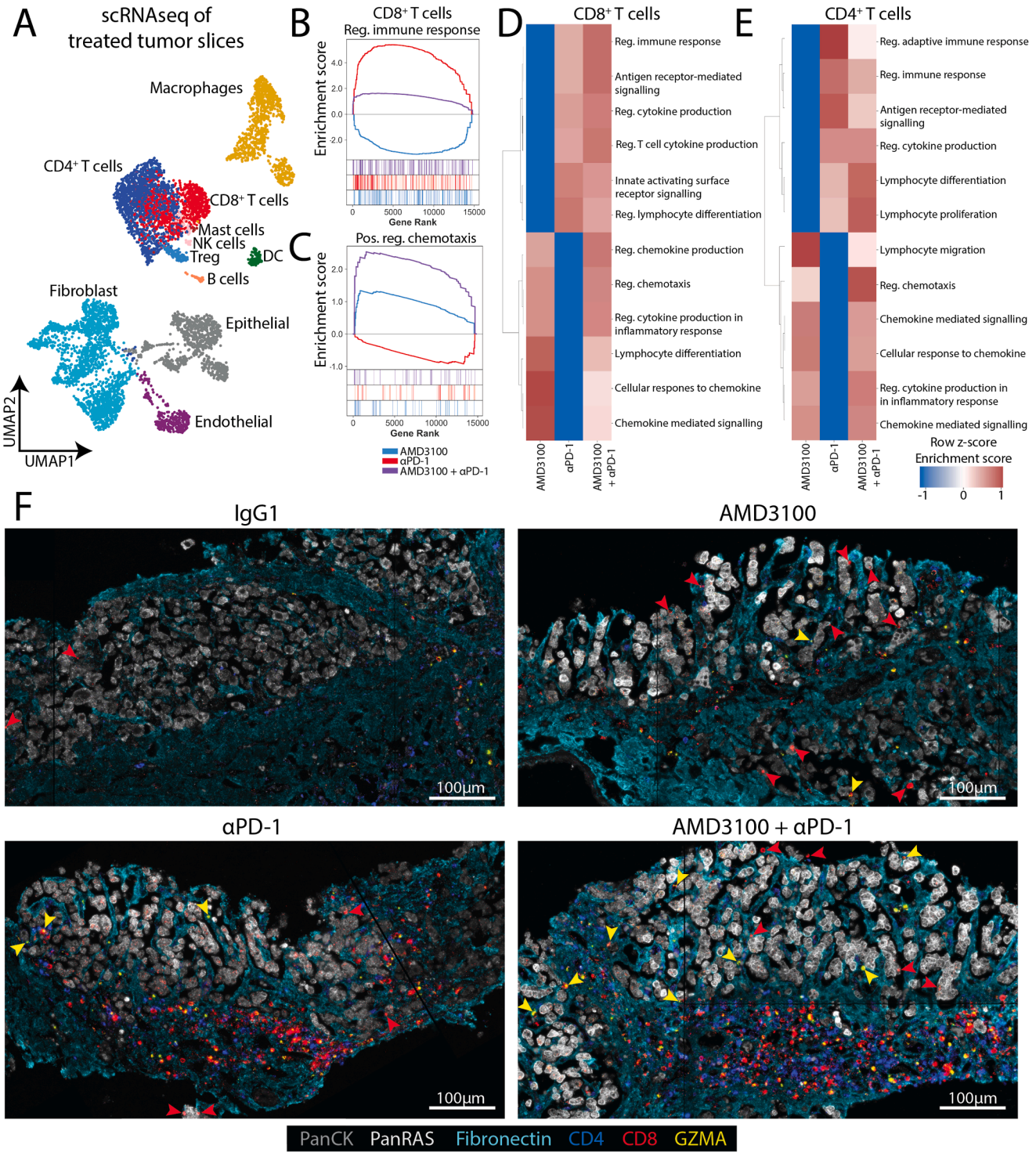

Figure 7. CXCR4 and PD-1 blockade function cooperatively to improve T-cell effector function. (*A*) UMAP showing single-cell sequencing data for TSCs taken from 1 patient and treated for 3 days with IgG1, CXCR4 inhibition (AMD3100), PD-1 blockade (α PD-1), or combination treatment (n = 6483 total cells). (*B*) Gene set enrichment analysis in $CD8^+$ T cells demonstrated increased expression of genes involved in immune response regulation after treatment with PD-1 blockade and (*C*) of positive regulation (pos. reg.) of chemotaxis after treatment with AMD3100. (*D*) Selected gene sets enriched following AMD3100, αPD-1, or combination treatment in $CD8^+$ cytotoxic T cells and (*E*) $CD4^+$ helper T cells. (*F*) Representative images of spatial proteomics data for tumor slice cultures from 1 patient sample treated with IgG1, AMD3100, α PD-1, or combination treatment for 3 days. *Dark gray*, panCK; *light gray*, panRAS (tumor cells); *cyan*, fibronectin (stroma); *blue*, CD4; *red*, CD8; *yellow*, GZMA. *Red and yellow arrowheads* highlight selected tumor-adjacent $CD8^+GZMA^-$ and $GZMA^+$ cells, respectively.

checkpoint inhibition has been unable to generate consistent antitumor immunity for these patients. We hypothesized that 2 distinct mechanisms are responsible for mediating immunosuppression in FLC: T-cell exclusion from the carcinoma compartment and immune checkpoint-mediated inhibition of TILs. To our knowledge, we have provided the first evidence that the CXCR4 pathway is a key mediator of FLC's characteristic lymphocyte sequestration. We used a TSC model to experimentally modulate the human FLC TIME, demonstrating that CXCR4 and PD-1 blockade work through independent mechanisms to cooperatively increase tumor cell death. Specifically, our results show that CXCR4 blockade promotes T-cell migration from stroma into the tumor and that PD-1 blockade increases activation of these mobilized lymphocytes.

The role of CXCL12-CXCR4 signaling as a poor prognostic marker and its importance in mediating lymphocyte tumor-infiltration and metastasis has been well-established in other tumor types.[43–46] In mouse models of PDAC, for example, depletion of FAP^+ CAFs was sufficient to induce antitumor immunity.[47] Subsequent work has demonstrated that the immunosuppressive effect of these myCAFs is mediated through CXCL12 and can be therapeutically reversed by CXCR4 inhibition.[34–36] Although the CXCL12-CXCR4 interaction acts in a chemoattractant manner in vitro to inhibit immune cell migration directed by many other chemokines, dimeric CXCL12 captured onto the surface of tumor cells expressing a KRT19 coat may instead result in the arrest of T-cell migration toward tumor cells.[34,35] Although fibroblasts are similarly the dominant source of CXCL12 in FLC, FLC tumor cells do not characteristically display a KRT19-CXCL12 coat. Our findings are overall consistent with a KRT19-independent CXCL12-CXCR4 interaction between stromal fibroblasts and lymphocytes resulting in a chemoattractive effect within the FLC TIME, potentially reflecting differences in monomeric vs dimeric forms of CXCL12.[34,48] Intriguingly, our live imaging experiments suggest that the effect of CXCR4 inhibition occurs rapidly and on a similar timescale to the mobilization of hematopoietic progenitors from the bone marrow by blocking chemoattractive CXCL12-CXCR4 signalling.[49] Additional work will need to clarify the roles of the CXCL12 complexed to KRT19 on cholangiocytes and of CXCL12-expressing endothelial cells, which have been shown to mediate immunosuppression through the recruitment of myeloid-derived suppressor cells in a mouse model of hepatocellular carcinoma.[50]

Despite these potential differences in the mechanisms of CXCL12-CXCR4 signaling-dependent T-cell exclusion across tumor types, our study similarly demonstrates that CXCR4 inhibition targets immune exclusion from the TIME and works in a synergistic manner with immune checkpoint blockade in the FLC TIME. Applying several orthogonal approaches to human FLC TSCs, including immunohistochemistry, living tissue microscopy, single-cell sequencing, and one of the first applications of highly multiplexed spatial proteomics to human tumor slices treated ex vivo, we have shown that CXCR4 and PD-1 blockade act through both $CD4^+$ and $CD8^+$ T cells to independently increase migration of stromal T cells into the carcinoma compartment and activate intratumoral T-cell effector function, respectively. Notably, because our TSC is derived only from tumor core specimens, in vivo CXCR4 blockade may result in even greater immune mobilization from T cells at the liver-tumor interface and from ANTL. Further work is needed to directly confirm that the observed increase in tumor cell death after combination therapy is T-cell–dependent, as shown in PDAC,[34–36,51] and to explore the role of other CXCR4 ligands that are also inhibited by AMD3100, such as multiplex immunofluorescent imaging.[21] The use of in vivo animal models to test combination CXCR4 and PD-1 blockade may ultimately be able to aid in further deciphering these FLC-specific mechanisms, however, current FLC mouse models are limited by their low penetrance, long growth times, and crucially the lack of FLC's characteristic stroma.[52–54] The complex role of CXCR4 signaling in other immune cell types, which includes both lymphocyte and myeloid populations, and thereby the ability of this combination immunotherapy strategy to promote an integrated immune response similarly remain incompletely understood.[55,56]

In conclusion, FLC remains an aggressive and difficult-to-treat liver cancer in adolescents and young adults. With therapeutic targeting of the immunogenic DNAJ-PKAc fusion kinase of particular interest, the development of new immunotherapies in this tumor type will need to additionally address FLC's characteristic stromal lymphocyte sequestration and intratumoral immunosuppression. Our results provide a valuable snRNAseq resource to parse the unique FLC TIME and establish a rational combination immunotherapy approach to target 2 independent immunosuppressive mechanisms in FLC, laying the preclinical groundwork for future clinical trials. Finally, our findings demonstrate the versatility of the TSC platform as an experimental system to understand the human TIME, particularly in rare cancer types.

Supplementary Material

Note: To access the supplementary material accompanying this article, visit the online version of *Gastroenterology* at www.gastrojournal.org, and at https://doi.org/10.1053/j.gastro.2025.10.006.

References

1. Kaseb AO, Shama M, Sahin IH, et al. Prognostic indicators and treatment outcome in 94 cases of fibrolamellar hepatocellular carcinoma. Oncology 2013; 85:197–203.
2. Aziz H, Brown ZJ, Panid Madani S, et al. Fibrolamellar hepatocellular carcinoma: comprehensive review of diagnosis, imaging, and management. J Am Coll Surg 2023;236:399–410.
3. O'Neill AF, Church AJ, Perez-Atayde AR, et al. Fibrolamellar carcinoma: an entity all its own. Curr Probl Cancer 2021;45:100770.
4. **Chen KY**, **Popovic A**, Hsiehchen D, et al. Clinical outcomes in fibrolamellar hepatocellular carcinoma treated

with immune checkpoint inhibitors. Cancers (Basel) 2022;14:5347.
5. Berger R, Dinstag G, Tirosh O, et al. Fibrolamellar carcinoma transcriptomic-based treatment prediction: complete response after nivolumab and ipilimumab. J Immunother Cancer 2022;10:e005620.
6. Toni EN De, Roessler D. Using dual checkpoint blockade to treat fibrolamellar hepatocellular carcinoma. Gut 2020;69:2056–2058.
7. Bauer U, Mogler C, Braren RF, et al. Progression after immunotherapy for fibrolamellar carcinoma. Visc Med 2019;35:39–42.
8. Darcy DG, Chiaroni-Clarke R, Murphy JM, et al. The genomic landscape of fibrolamellar hepatocellular carcinoma: whole genome sequencing of ten patients. Oncotarget 2015;6:755–770.
9. **Dinh TA**, **Utria AF**, **Barry KC**, et al. A framework for fibrolamellar carcinoma research and clinical trials. Nat Rev Gastroenterol Hepatol 2022;19:328–342.
10. **Honeyman JN**, **Simon EP**, **Robine N**, et al. Detection of a recurrent DNAJB1-PRKACA chimeric transcript in fibrolamellar hepatocellular carcinoma. Science (1979) 2014;343:1010–1014.
11. Graham RP, Torbenson MS. Fibrolamellar carcinoma: a histologically unique tumor with unique molecular findings. Semin Diagn Pathol 2017;34:146–152.
12. Lalazar G, Simon S. Fibrolamellar carcinoma: recent advances and unresolved questions on the molecular mechanisms. Semin Liver Dis 2018;38:051–059.
13. Bauer J, Köhler N, Maringer Y, et al. The oncogenic fusion protein DNAJB1-PRKACA can be specifically targeted by peptide-based immunotherapy in fibrolamellar hepatocellular carcinoma. Nat Commun 2022;13:6401.
14. Kirk AM, Crawford JC, Chou C-H, et al. DNAJB1-PRKACA fusion neoantigens elicit rare endogenous T cell responses that potentiate cell therapy for fibrolamellar carcinoma. Cell Rep Med 2024;5:101469.
15. **Daniel SK**, **Sullivan KM**, Dickerson LK, et al. Reversing immunosuppression in the tumor microenvironment of fibrolamellar carcinoma via PD-1 and IL-10 blockade. Sci Rep 2024;14:5109.
16. Kim AK, Gani F, Layman AJ, et al. Multiple immunesuppressive mechanisms in fibrolamellar carcinoma. Cancer Immunol Res 2019;7:805–812.
17. Kenerson HL, Sullivan KM, Labadie KP, et al. Protocol for tissue slice cultures from human solid tumors to study therapeutic response. STAR Protoc 2021;2:100574.
18. Kenerson HL, Sullivan KM, Seo YD, et al. Tumor slice culture as a biologic surrogate of human cancer. Ann Transl Med 2020;8:114.
19. Jiang X, Seo YD, Chang JH, et al. Long-lived pancreatic ductal adenocarcinoma slice cultures enable precise study of the immune microenvironment. Oncoimmunology 2017;6:e1333210.
20. Jiang X, Seo YD, Sullivan KM, et al. Establishment of slice cultures as a tool to study the cancer immune microenvironment. In: Methods in Molecular Biology. New York: Humana Press, 2019:283–295.
21. Farghli AR, Chan M, Sherman MS, et al. Single-cell multi-omic analysis of fibrolamellar carcinoma reveals rewired cell-to-cell communication patterns and unique vulnerabilities. bioRxiv 2024;2024.12.11.627911.
22. Requena D, Medico JA, Soto-Ugaldi LF, et al. Liver cancer multiomics reveals diverse protein kinase A disruptions convergently produce fibrolamellar hepatocellular carcinoma. Nat Commun 2024;15:10887.
23. Jewell ML, Gibson JR, Guy CD, et al. Single-cell RNA sequencing identifies yes-associated protein 1–dependent hepatic mesothelial progenitors in fibrolamellar carcinoma. Am J Pathol 2020;190:93–107.
24. Long D, Chan M, Han M, et al. Proteo-metabolomics and patient tumor slice experiments point to amino acid centrality for rewired mitochondria in fibrolamellar carcinoma. Cell Rep Med 2024;5:101699.
25. Ma RK, Tsai P-Y, Farghli AR, et al. DNAJB1-PRKACA fusion protein-regulated LINC00473 promotes tumor growth and alters mitochondrial fitness in fibrolamellar carcinoma. PLoS Genet 2024;20:e1011216.
26. Dinh TA, Sritharan R, Smith FD, et al. Hotspots of aberrant enhancer activity in fibrolamellar carcinoma reveal candidate oncogenic pathways and therapeutic vulnerabilities. Cell Rep 2020;31:107509.
27. Dinh TA, Vitucci ECM, Wauthier E, et al. Comprehensive analysis of The Cancer Genome Atlas reveals a unique gene and non-coding RNA signature of fibrolamellar carcinoma. Sci Rep 2017;7:44653.
28. **Malouf GG**, **Job S**, Paradis V, et al. Transcriptional profiling of pure fibrolamellar hepatocellular carcinoma reveals an endocrine signature. Hepatology 2014;59:2228–2237.
29. Guo F, Wang Y, Liu J, et al. CXCL12/CXCR4: a symbiotic bridge linking cancer cells and their stromal neighbors in oncogenic communication networks. Oncogene 2016;35:816–826.
30. Zhou W, Guo S, Liu M, et al. Targeting CXCL12/CXCR4 axis in tumor immunotherapy. Curr Med Chem 2019; 26:3026–3041.
31. Kohli K, Pillarisetty VG, Kim TS. Key chemokines direct migration of immune cells in solid tumors. Cancer Gene Ther 2022;29:10–21.
32. Sun X, Cheng G, Hao M, et al. CXCL12 / CXCR4 / CXCR7 chemokine axis and cancer progression. Cancer Metastasis Rev 2010;29:709–722.
33. **Dickerson LK**, **Carter JA**, Kohli K, et al. Emerging interleukin targets in the tumour microenvironment: implications for the treatment of gastrointestinal tumours. Gut 2023;72:1592–1606.
34. Wang Z, Moresco P, Yan R, et al. Carcinomas assemble a filamentous CXCL12–keratin-19 coating that suppresses T cell–mediated immune attack. Proc Natl Acad Sci 2022;119: e2119463119.
35. **Biasci D**, **Smoragiewicz M**, **Connell CM**, et al. CXCR4 inhibition in human pancreatic and colorectal cancers induces an integrated immune response. Proc Natl Acad Sci 2020;117:28960–28970.
36. **Feig C**, **Jones JO**, **Kraman M**, et al. Targeting CXCL12 from FAP-expressing carcinoma-associated fibroblasts synergizes with anti–PD-L1 immunotherapy in pancreatic cancer. Proc Natl Acad Sci 2013;110:20212–20217.
37. Ward SC, Huang J, Tickoo SK, et al. Fibrolamellar carcinoma of the liver exhibits immunohistochemical

evidence of both hepatocyte and bile duct differentiation. Mod Pathol 2010;23:1180–1190.
38. Cornella H, Alsinet C, Sayols S, et al. Unique genomic profile of fibrolamellar hepatocellular carcinoma. Gastroenterology 2015;148:806–818.e10.
39. Seo YD, Jiang X, Sullivan KM, et al. Mobilization of CD8+ T cells via CXCR4 blockade facilitates PD-1 checkpoint therapy in human pancreatic cancer. Clin Cancer Res 2019;25:3934–3945.
40. Hatse S, Princen K, Bridger G, et al. Chemokine receptor inhibition by AMD3100 is strictly confined to CXCR4. FEBS Lett 2002;527:255–262.
41. Veldman-Jones MH, Brant R, Rooney C, et al. Evaluating robustness and sensitivity of the NanoString Technologies nCounter Platform to enable multiplexed gene expression analysis of clinical samples. Cancer Res 2015;75:2587–2593.
42. **Subramanian A**, **Tamayo P**, Mootha VK, et al. Gene set enrichment analysis: a knowledge-based approach for interpreting genome-wide expression profiles. Proc Natl Acad Sci 2005;102:15545–15550.
43. Shi Y, Riese DJ, Shen J. The Role of the CXCL12/CXCR4/CXCR7 chemokine axis in cancer. Front Pharmacol 2020;11:574667.
44. Mortezaee K. CXCL12/CXCR4 axis in the microenvironment of solid tumors: a critical mediator of metastasis. Life Sci 2020;249:117534.
45. **Domanska UM, Kruizinga RC**, Nagengast WB, et al. A review on CXCR4/CXCL12 axis in oncology: no place to hide. Eur J Cancer 2013;49:219–230.
46. Daniel SK, Seo YD, Pillarisetty VG. The CXCL12-CXCR4/CXCR7 axis as a mechanism of immune resistance in gastrointestinal malignancies. Semin Cancer Biol 2020;65:176–188.
47. **Kraman M**, **Bambrough PJ**, **Arnold JN**, et al. Suppression of antitumor immunity by stromal cells expressing fibroblast activation protein–α. Science 2010;330:827–830.
48. **Moresco P**, **Kastan JP**, Yang J, et al. Signal peptide-independent secretion of keratin-19 by pancreatic cancer cells. Proc Natl Acad Sci 2025;122:e2426218122.
49. **Dar A**, **Schajnovitz A**, **Lapid K**, et al. Rapid mobilization of hematopoietic progenitors by AMD3100 and catecholamines is mediated by CXCR4-dependent SDF-1 release from bone marrow stromal cells. Leukemia 2011;25:1286–1296.
50. **Lu Y**, **Liu Y**, **Zuo X**, et al. CXCL12+ tumor-associated endothelial cells promote immune resistance in hepatocellular carcinoma. J Hepatol 2025;82:634–648.
51. Bockorny B, Semenisty V, Macarulla T, et al. BL-8040, a CXCR4 antagonist, in combination with pembrolizumab and chemotherapy for pancreatic cancer: the COMBAT trial. Nat Med 2020;26:878–885.
52. Kastenhuber ER, Lalazar G, Houlihan SL, et al. DNAJB1-PRKACA fusion kinase interacts with β-catenin and the liver regenerative response to drive fibrolamellar hepatocellular carcinoma. Proc Natl Acad Sci U S A 2017;114:13076–13084.
53. Engelholm LH, Riaz A, Serra D, et al. CRISPR/Cas9 engineering of adult mouse liver demonstrates that the Dnajb1–Prkaca gene fusion is sufficient to induce tumors resembling fibrolamellar hepatocellular carcinoma. Gastroenterology 2017;153:1662–1673.e10.
54. He A, Coles GL, Hartmann GG, et al. Development of pre-clinical murine models for fibrolamellar hepatocellular carcinoma. bioRxiv 2023;2023.12.06.569624.
55. Morita S, Lei P-J, Shigeta K, et al. Combination CXCR4 and PD-1 blockade enhances intratumoral dendritic cell activation and immune responses against hepatocellular carcinoma. Cancer Immunol Res 2025;13:162–170.
56. **Damle SR, Carter JA**, Goodsell KG, et al. Intratumoral three-cell-type clusters are a conserved feature of endogenous antitumor immunity. Cancer Immunol Res 2026;14:205–218.

Author names in bold designate shared co-first authorship.

Received June 3, 2025. Accepted October 2, 2025.

Correspondence
Address correspondence to: Venu G. Pillarisetty, MD, University of Washington, 1959 NE Pacific Street, Box 356410, Seattle, Washington 98195. e-mail: vgp@uw.edu; or Praveen Sethupathy, PhD, Cornell University College of Veterinary Medicine, T7 006D Veterinary Research Tower, Box 17, Ithaca, New York 14853. e-mail: pr46@cornell.edu.

Acknowledgments
The authors would like to acknowledge the following individuals and groups: Stephanie Weaver, David Sierra, and Amanda Koehne of the Fred Hutch Cancer Center Experimental Histopathology Core; the Fred Hutch Cancer Center Genomics Core, including Katie Kim, Alex Zevin, and Dolores Covarrubias; Pamela Yang for assistance with RNA extraction; Kaitlyn LaCourse for Nanostring analysis support; James Li and Kelly Hudkins of the University of Washington Pathology Research Lab; Nathaniel Peters and the W.M. Keck Microscopy Center; Wai Pang Chan and Mark Headley for additional live microscopy insight; and Patrick Heagerty and the University of Washington Institute of Translational Health Sciences biostatistical services for support with statistical analysis.

CRediT Authorship Contributions
Jason A. Carter, MD, PhD (Conceptualization: Equal; Data curation: Equal; Formal analysis: Equal; Investigation: Equal; Methodology: Equal; Software: Equal; Writing – original draft: Equal; Writing – review & editing: Equal)
Lindsay K. Dickerson, MD (Conceptualization: Equal; Data curation: Equal; Formal analysis: Equal; Investigation: Equal; Methodology: Equal; Visualization: Equal; Writing – original draft: Equal; Writing – review & editing: Equal)
Andreas Stephanou, BS (Data curation: Equal; Formal analysis: Equal; Investigation: Equal; Methodology: Equal; Software: Equal; Writing – review & editing: Equal)
Sheela R. Damle, MD, PhD (Data curation: Supporting; Formal analysis: Supporting; Methodology: Supporting; Writing – review & editing: Supporting)
Kristin E. Goodsell, MD (Data curation: Supporting; Formal analysis: Supporting; Methodology: Supporting; Writing – review & editing: Supporting)
Sara K. Daniel, MD (Investigation: Supporting; Methodology: Supporting; Writing – review & editing: Supporting)
Kevin M. Sullivan, MD (Investigation: Supporting; Methodology: Supporting; Writing – review & editing: Supporting)
Bo Shui, PhD (Investigation: Supporting; Methodology: Supporting; Writing – review & editing: Supporting)
Xiuyun Jiang, PhD (Data curation: Supporting; Investigation: Supporting; Methodology: Supporting; Writing – review & editing: Supporting)
Heidi L. Kenerson, MS (Data curation: Supporting; Investigation: Supporting; Methodology: Supporting; Writing – review & editing: Supporting)
Renske van den Bijgaart, PhD (Investigation: Supporting; Methodology: Supporting; Writing – review & editing: Supporting)
Alaa Farghli, PhD (Investigation: Supporting; Methodology: Supporting; Software: Supporting; Writing – review & editing: Supporting)
Yongjun Liu, MD (Investigation: Supporting; Methodology: Supporting; Writing – review & editing: Supporting)
Emily Beirne, MS (Investigation: Supporting; Methodology: Supporting; Writing – review & editing: Supporting)
Kevin P. Labadie, MD (Investigation: Supporting; Writing – review & editing: Supporting)
Jack Cernak, BS (Investigation: Supporting; Methodology: Supporting; Writing – review & editing: Supporting)
Sardar Shahmir Chauhan, MBBS (Investigation: Supporting; Writing – review & editing: Supporting)

Jose Mario Bello Pineda, MD, PhD (Investigation: Supporting; Writing – review & editing: Supporting)
Annalyssa N. Long, BS (Investigation: Supporting; Methodology: Supporting; Writing – review & editing: Supporting)
Anna E. Elz, MSc (Investigation: Supporting; Methodology: Supporting; Writing – review & editing: Supporting)
Evan N. Newell, PhD (Methodology: Supporting; Writing – review & editing: Supporting)
Teresa S. Kim, MD (Investigation: Supporting; Methodology: Supporting; Supervision: Supporting; Writing – review & editing: Supporting)
Kimberly J. Riehle, MD (Methodology: Supporting; Supervision: Supporting; Writing – review & editing: Supporting)
Raymond Yeung, MD (Methodology: Supporting; Supervision: Supporting; Writing – review & editing: Supporting)
Shreeram Akilesh, MD (Methodology: Supporting; Supervision: Supporting; Writing – review & editing: Supporting)
Ian N. Crispe, MBBS, PhD (Conceptualization: Supporting; Methodology: Supporting; Supervision: Supporting; Writing – review & editing: Supporting)
Kevin C. Barry, PhD (Investigation: Supporting; Methodology: Supporting; Supervision: Supporting; Writing – review & editing: Supporting)
Praveen Sethupathy, PhD (Conceptualization: Supporting; Data curation: Supporting; Formal analysis: Supporting; Funding acquisition: Supporting; Methodology: Supporting; Software: Supporting; Supervision: Supporting; Writing – review & editing: Supporting)
Venu G. Pillarisetty, MD (Conceptualization: Supporting; Data curation: Supporting; Formal analysis: Supporting; Funding acquisition: Lead; Investigation: Supporting; Methodology: Supporting; Project administration: Supporting; Supervision: Lead; Writing – review & editing: Supporting)

Conflicts of interest

This author discloses the following: Venu G. Pillarisetty has previously served as a member of the scientific advisory board for TriSalus Life Sciences (2022-2024) and as a consultant for Merck & Company (2018), GlaxoSmithKline (2019), Imvax (2019), Takeda (2020), and Umoja (2022); and has previously had research funding from AstraZeneca, Ipsen, Merck, OncoResponse, and NGM. The funders had no role in the conceptualization, design, data collection, analysis, decision to publish, or preparation of the manuscript. The remaining authors disclose no conflicts.

Funding

This research was supported by The Fibrolamellar Cancer Foundation (separate awards to V.G.P. and P.S.), the Department of Defense (CA180067 to V.G.P. and R.S.Y.), and a Department of Defense Career Development Award (CA230890 to J.A.C.). The Experimental Histopathology Shared Resource of the Fred Hutch/University of Washington Cancer Consortium was supported by the National Institutes of Health (P30 CA015704) and the University of Washington Keck Microscopy Center was supported by the National Institutes of Health (S10 OD016240), as well as the University of Washington Student Technology Fee. L.K.D. and K.M.S. were recipients of Cancer Research Institute/Fibrolamellar Cancer Foundation Postdoctoral Fellowships (CRI Award 4093).

Data Availability

RNA sequencing data has been deposited in the Gene Expression Omnibus repository under accession GSE306436. Processed data and associated data analysis code are freely available at: https://github.com/JasonACarter/FLC_CXCR4_Gastro2025.